Andean Geology 42 (1): 36-55. January, 2015
doi: 10.5027/andgeoV42n1-a03

Andean Geology
www.andeangeology.cl

Counterclockwise post-emplacement evolution of metatroctolites from Aluminé Igneous-Metamorphic Complex, Neuquén, Argentina.

Ivana Urraza[1, 3], Sergio Delpino[1, 2], Laura Grecco[2]

[1] *Departamento de Geología, Universidad Nacional del Sur, San Juan 670, Bahía Blanca, Argentina. iurraza@uns.edu.ar; sdelpino@criba.edu.ar*

[2] *Instituto Geológico del Sur, CONICET-Universidad Nacional del Sur, San Juan 670, Bahía Blanca, Argentina. mlgrecco@criba.edu.ar*

[3] *Departamento de Geología y Petróleo, Facultad de Ingeniería, Universidad Nacional del Comahue, Buenos Aires 1400, 830 Neuquén, Argentina.*

ABSTRACT. Post-crystallization evolution of the metatroctolites of the Ñorquinco lake zone, Aluminé Igneous-Metamorphic Complex, is analyzed. These mafic rocks show coronas around olivine, composed of Opx, Cpx, Spl and Amp (Hbl_1 and Hbl_2). The temporal evolution of these rocks was evaluated via petrographic analysis and the construction of a suitable pseudosection based on the whole-rock chemical composition. This analysis was complemented with classic geothermobarometry, from which four stages on the P-T path were established: **A.** Starting point lies in the stability field of the Pl-Ol-Opx-Cpx-H_2O, with P-T of 936 ºC and 2.7 kbar, respectively, indicative of granulite facies conditions; **B.** Another point in the trajectory is represented by first appearance of amphibole. P-T conditions for Hbl_1-Pl are 780 °C and 5.9 Kbar, respectively.; **C.** The third point is characterized by the presence of Hbl_2 and Spl and the disappearance of Ol, leading to the association Pl-Opx-Cpx-Hbl_2-Spl-H_2O. Equilibrium temperature and pressure for this stage are 780 ºC and 5.69 Kbar, respectively; and **D.** The last point in the path implies the disappearance of Cpx and the retrogression of the phases to Chl with, a concomitant consumption of excess water. Both the equilibrium temperature (694.2 ºC) for the stable association Pl-Opx-Hbl_2-Spl-Chl, and the narrow stability pressure range (4.5-5.2 Kbar), are constrained by the absence of olivine and garnet. The defined portion of the P-T path indicates cooling from granulite to amphibolite facies with a concomitant pressure increment, defining a counter-clockwise P-T path. U-Pb zircon ages determined for basement xenoliths in metatroctolites and gabbroic inclusions in granodiorites, allows constraining the emplacement of Ñorquinco lake metatroctolites to Upper Paleozoic times.

Keywords: Metatroctolites, Aluminé Igneous-Metamorphic Complex, Reaction coronas, Geothermobarometry, P-T path.

RESUMEN. Evolución antihoraria posemplazamiento de las metatroctolitas del Complejo Ígneo-Metamórfico Aluminé, Neuquén, Argentina. El objetivo de este trabajo es analizar la evolución poscristalización de cuerpos máficos que afloran en la zona de lago Ñorquinco (sector sur del Complejo Ígneo Metamórfico Aluminé), los cuales han sido clasificados como metatroctolitas. Estas rocas muestran coronas de reacción alrededor del olivino que resultan del reequilibrio posmagmático, compuestas principalmente de Opx, Cpx, Spl y Amp (Hbl_1 y Hbl_2). La evolución temporal de las metatroctolitas fue evaluada a partir de relaciones de fase determinadas a partir del análisis petrográfico y de la construcción de una pseudosección adecuada basada en la composición química de la roca total. Este análisis fue complementado con estudios de geotermobarometría clásica, a partir de los cuales se establecieron cuatro estadios sobre una trayectoria P-T: **A.** El punto de inicio para la retrogresión se ubica en el campo de estabilidad de la asociación Pl-Ol-Opx-Cpx-H_2O, en condiciones de P-T de 936 ºC y 2,7 kbar en facies de granulita; **B.** El segundo estadio sobre la trayectoria está representado por la presencia de anfíbol en condiciones de P-T de 780 ºC y 5,69 kbar para la estabilidad del par Hbl_1-Pl; **C.** El tercer punto en la trayectoria P-T está caracterizado por la aparición de Hbl_2 y Spl y la desaparición de Ol, lo que conduce a la asociación estable Pl-Opx-Cpx-Hbl_2-Spl- H_2O. Las temperaturas y presiones de equilibrio para este estadio son de 780 ºC y 5,69 Kbar; y **D.** El último punto definido implica la desaparición de Cpx y la retrogradación de las fases a Chl con un consumo concomitante de agua en exceso. Tanto la temperatura de equilibrio (694,2 ºC) para la asociación estable Pl-Opx-Hbl_2-Spl-Chl, como el rango estrecho de la presión de estabilidad (4,5-5,2 Kbar) son limitado por la ausencia de olivino y granate. La trayectoria P-T definida indica enfriamiento a partir de granulita a facies de anfibolita con un incremento concomitante con la presión, definiendo una trayectoria P-T antihoraria. Edades U-Pb en circones determinadas para xenolitos de basamento en las metatroctolitas e inclusiones gabroides en granodioritas, permiten delimitar el emplazamiento de las metatroctolitas del lago Ñorquinco al Paleozoico Superior.

Palabras clave: Metatroctolitas, Complejo Ígneo-Metamórfico Aluminé, Coronas de reacción, Geotermobarometría, Trayectoria P-T.

1. Introduction

In the southern region of the Aluminé Igneous-Metamorphic Complex (AIMC) (Urraza *et al*., 2008a and b, 2009, 2011; Urraza, 2014), mafic bodies of variable dimensions are emplaced in a metapelitic sequence composed by schists, gneisses and amphibolites. This sequence of pre-Andean rocks constitutes an accretionary prism related to the subduction of the oceanic plate, bellow the southwestern Gondwana margin during the Paleozoic (Urraza, 2014). Mafic bodies represented by metanorites and metatroctolites, are distributed along the Ñorquinco and Pulmarí lakes (Fig. 1A). The Ñorquinco metatroctolites constitute the northernmost outcrops of metamafic rocks, and are characterized by the presence of coronas developed around relict-magmatic olivine crystals and different replacement textures involving amphiboles. The formation of coronas, reaction rims and symplectites indicates changes in chemical and/or physical factors. These changes can take place either during a prograde or a retrograde metamorphic event, and are sometimes associated with cooling from igneous temperatures (*e.g*., Griffin and Heier, 1973; Mongkoltip and Ashworth 1983). Kelyphytic corona textures and different types of symplectites are common in gabbros, also in metatroctolites regarding to reactions between olivine and plagioclase (Claeson, 1998; Lang *et al*., 2004). These microstructures always present great interest as they provide invaluable information in the reconstruction of the metamorphic evolution and P-T conditions of the rocks (Cruciani *et al*., 2008).

There are many examples in literature of reaction textures, coronas and symplectites; some of them were given in: cumulates in NE Sardinia, Italia (Franceschelli *et al*., 2002); in metatroctolites from Buchcreek, North Carolina Blue Ridge (Lang *et al*., 2004); in Rymmen gabbro from Southern Sweden (Cleason, 1998); in gabbros from Black Hill, South Australia (Turner and Stüwe, 1992); in troctolitic gabbros in Norway (Ashworth, 1986), among others. In Argentina, there are some examples in mafic rocks from Sierras de San Luis (Cruciani *et al*., 2008, 2011, 2012; Brogioni *et al*., 2007) and in Sierra del Valle Fértil and La Huerta (Otamendi *et al*., 2010; Gallien *et al*., 2012). This contribution constitutes the first mention of mafic coronitic rocks outside the Sierras Pampeanas context.

This study was focused on metatroctolites that exhibit coronas between olivine and plagioclase, and involve the analysis of mineral assemblages, textures, microstructures, whole-rock/mineral geochemistry, geochronology and metamorphic reactions, in order to define the P-T trajectory of the metatroctolites of Ñorquinco lake.

2. Geological Setting

The metatroctolites, previously denominated troctolitic metagabbros (Urraza *et al*., 2012, 2013; Urraza, 2014) form part of the Aluminé Igneous-Metamorphic Complex (AIMC), which has been defined as a set of intrusive-igneous pre-Andean and Andean rocks and its metamorphic country-rocks. The AIMC is located between the Aluminé, Moquehue, Ñorquinco and Pulmarí lakes, in the Neuquén province of Argentina (Urraza *et al*., 2008a, 2011). The AIMC forms the northern sector of the zone limited by the Pino Hachado-Picún Leufú (PH-PL) and Nahuel Huapi (NH) megalineaments, defined by Ramos (1978) as Aluminé Batholithic Belt (Fig. 1A).

The pre-Andean tectonic context for the AIMC, is represented in figure 1B. The AIMC is located within a complex tectonic framework. According to Vaughan and Pankhurst (2008), the sector between 38° and 40°S presents a high grade of complexity due to the scarcity of detailed information, from what they marked this area with a question mark. This zone limits to the north with the Chilean and Cuyanean terranes, whereas towards the south it is in contact with the North Patagonian Massif and Patagonia. The tectonic Andean frame also presents a high grade of complexity due to the successive emplacement of igneous bodies forming different batholiths. The Patagonian Batholith (PB), located between 38º30'S and 56ºS, records the Andean subducción initiation at around 150 Ma ago, in the Jurassic period (Hervé *et al*., 2007). The northern portion of the PB is named North Patagonian Batholith (NPB). Previously, Gordon and Ort (1993), had called Subcordilleran Patagonian Batholith (SCB) to the jurassic granitic rocks arranged in a NNE trend. Same authors named Cordilleran Patagonian Batholith (CPB) to the cretaceous granitic rocks distributed along the N-S direction (Fig. 1C). The locations of the Central Patagonian Batholith (CPB) and the Somuncurá Batholith (SB), are showed in figure 1C. In spite of in figure 1C outcrops of the PB and SCB are only showed to occur to the south of 40°S, rocks corresponding to these batholiths can be recognized up to the 38º30'S (Urraza *et al*., 2011).

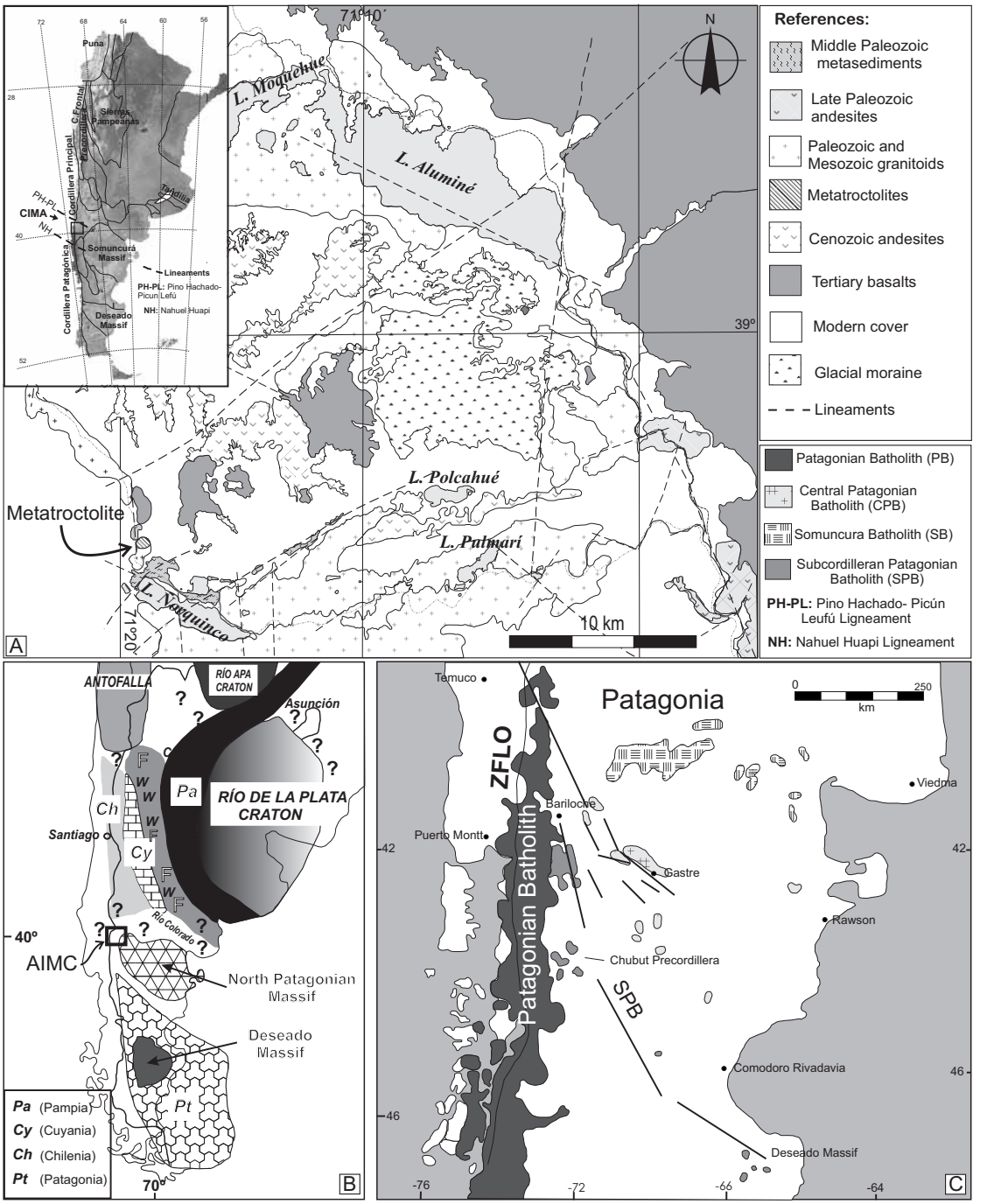

FIG. 1. Location and geologic setting for the AIMC. **A.** Geologic map of the AIMC showing the locations of the metatroctolites (modified after Urraza *et al*., 2011); **B.** Geologic pre-Andean frame (modified after Vaughan and Pankhurst, 2008). Note the locations of the study area in a key zone of convergence of several terranes, and which counts up to the present with very scarce geologic information; **C.** Modified scheme of Gordon and Ort (1993), showing the locus, dimensions and orientation of the bodies that conform the SCB and the PB south of the 40ºS. The locations of the CPB and SB, are also showed.

3. Country rocks

The metamorphic basement of the AIMC is represented by small isolated outcrops of quartzo-feldespatic metapelites and amphibolites. Most of the outcrops are constituted by gneisses intensely foliated, with injections of granitic material of the 'lit par lit' type and frequently showing isoclinal, intrafoliar and/or ptygmatic folding. With less representation, finely foliated amphibolites have been recognized (Fig. 2). These rocks also show thin injections of the 'lit par lit' type along the foliation planes and irregular granitic veins, usually of greater thicknesses, which cut the foliation

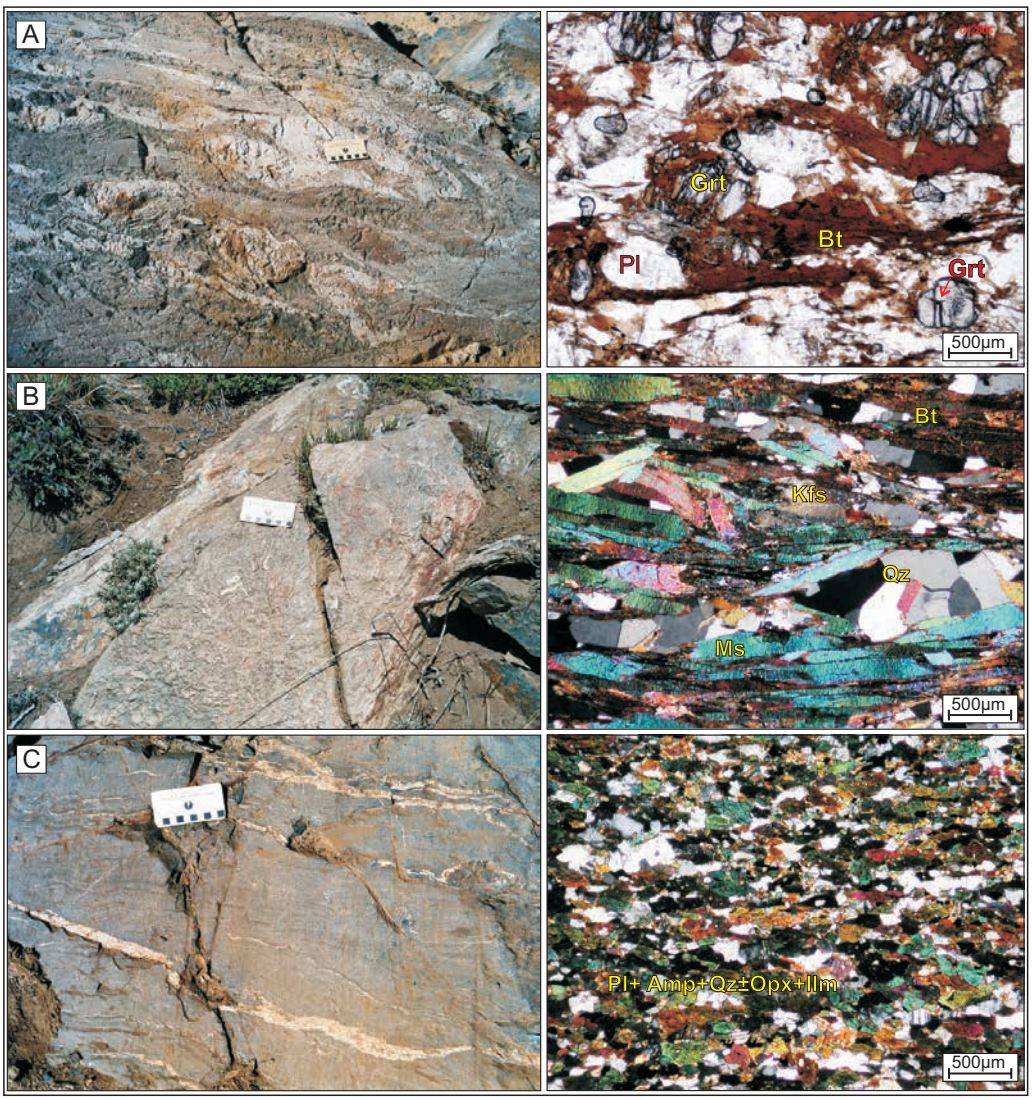

FIG. 2. The field characteristics of the different lithological types conforming country-rocks, are showed on the left side of the figure, whereas a microphotography corresponding to each of them are presented on the right. **A.** Injected gneisses: are composed of the association Qz+Pl+Ms+And±Bt±Grt+Zrn+Ap. Garnet, biotite and the fibrolitic sillimanite (this last one not observed in the microphotography due to the scale), form the anastomosed mylonitic foliation corresponding to the ductile deformation event that led to the intense recrystallization of quartz and moderate recrystallization of plagioclase; **B.** Muscovitic schists: present similar deformation to gneisses, showing development of polycrystalline quartz aggregates forming 120° triple junctions, surrounded by folia composed mainly of muscovite; **C.** Injected amphibolites: composed by hornblende and intensely recrystallized plagioclase.

with different angles (Urraza *et al*., 2009; Urraza, 2014). The varieties of basement described above correspond to *in situ* exposures, but they have been also observed as variable sized inclusions in gabbros and tonalites. Rarely and in thin strips, the gneissic basement loses partly its ptygmatic appearance and acquires a very well defined and very regularly orientated foliation. In this case, the foliation is marked by granitic thin injections, the stretching and boudinage of the thickest veins and by the distribution of abundant micas along the foliation planes. The loss of the intensely folded gneissic structure and the increase of phylosilicates in these bands, led to the rock to acquire a schistose appearance (Fig. 2B). The original metamorphic paragenesis of the injected gneisses is constituted by Qz+Pl+Ms+And±Bt±Grt+Zrn+Ap (Fig. 2A) (abbreviations after Withney and Evans, 2010). This association is stable at moderated to low temperatures (<620 ºC at X_{H2O}=1, or still lower at lower X_{H2O}) and pressures below 3.8 Kb. This early association is overprinted by a ductile deformation event that led to the intense recrystallization of quartz, moderate recrystallization of plagioclase and the development of an anastomosed mylonitic foliation (Fig. 2A). The geothermobarometry of the association stable during this deformation event (Bt+Grt+Sil(Fib)+opaque minerals), gave pressures and temperatures in the ranges 6.2-6.7 Kb and 605-620 ºC, respectively. The presence of sillimanite in these rocks require of minimum temperatures of 615 ºC at 6.2 Kb and 640 ºC at 6.7 Kb (Urraza *et al*., 2009). The injected amphibolites are composed of Qz+Pl+Hbl±Bt, plus accessories and opaque minerals. Amphibolites also show ductile deformation evidenced by intense recrystallization of plagioclase and amphibole, which underwent significant reduction of the grain size and development of pseudo-polygonal new grains meeting at 120° triple junctions. These fine aggregates arrange in folia, which together with the preferential orientation of relict crystals define the mylonitic foliation (Fig. 2C).

4. Field description of the metatroctolites

The studied metatroctolites show (at outcrop scale) a fine granular texture in the borders of the body that increases progressively in size towards the center, where it develops a coarse to very coarse granular texture (Fig. 3). This rocks show an anastomosed penetrative foliation with a general SSW trend (mean: 200º/80º DD/D) (Fig. 3D).

However, these rocks show a widespread retrogression, the magmatic mineralogical association can be still recognized in some thin sections. The intrusive body contains inclusions of the surrounding metamorphic basement, whose mineral associations and textures have been strongly obliterated (Figs. 3B and C). Regarding mineralogy of these basement inclusions, only quartz and intensely altered plagioclase and biotite are preserved, and the primitive foliation is only marked by the preferred orientation of quartz ribbons. The body of metatroctolites is cut by aplitic dikes of up to 60 cm thickness oriented 130º/66° (dip direction/dip) and coarse pegmatitic dikes in which stand out perhitic K-feldspar crystals of up to 10 cm and tourmaline (Figs. 3A and E).

5. Geochemistry and classification

A detailed sampling traversing the whole gabbroic body including 11 samples were carried out, in order to asses the structural, textural and compositional variations. Geochemical analysis including major and trace elements, were performed in the Actlabs laboratory, Canada, using ICP-MS. For the classification of the original magmatic rock and the geothermobarometric analysis, samples of the center of the body which better preserve the magmatic (texture and mineralogical composition) and metamorphic characteristics (post-crystallization textures and minerals), were selected.

The representative geochemical composition of metatroctolites is presented in Table 1. According to its SiO_2 content (43.1%), this rock is located close to the limit between basic and ultrabasic rocks following the Le Maitre (1989) silica content classification. Taking into account that the mineral proportions of ferromagnesian minerals in the studied metatroctolites are significantly lower than 90%, these rocks are considered to be mafic. The alkalis sum (Na_2O+K_2O=0.71) and calcium content (11.62%), point to a sub-alkaline signature. In addition, this magnesian-rock presents an X_{Mg}=0.73 (in atomic proportions) and very low TiO_2 (0.068%). Considering its chemical and mineralogical composition, these metatroctolites can be compared with gabbronorites and gabbroic inclusions in granodiorites found in the same sector of the AIMC. The above mentioned rocks with SiO_2 contents in the range 48.38-51.65% and

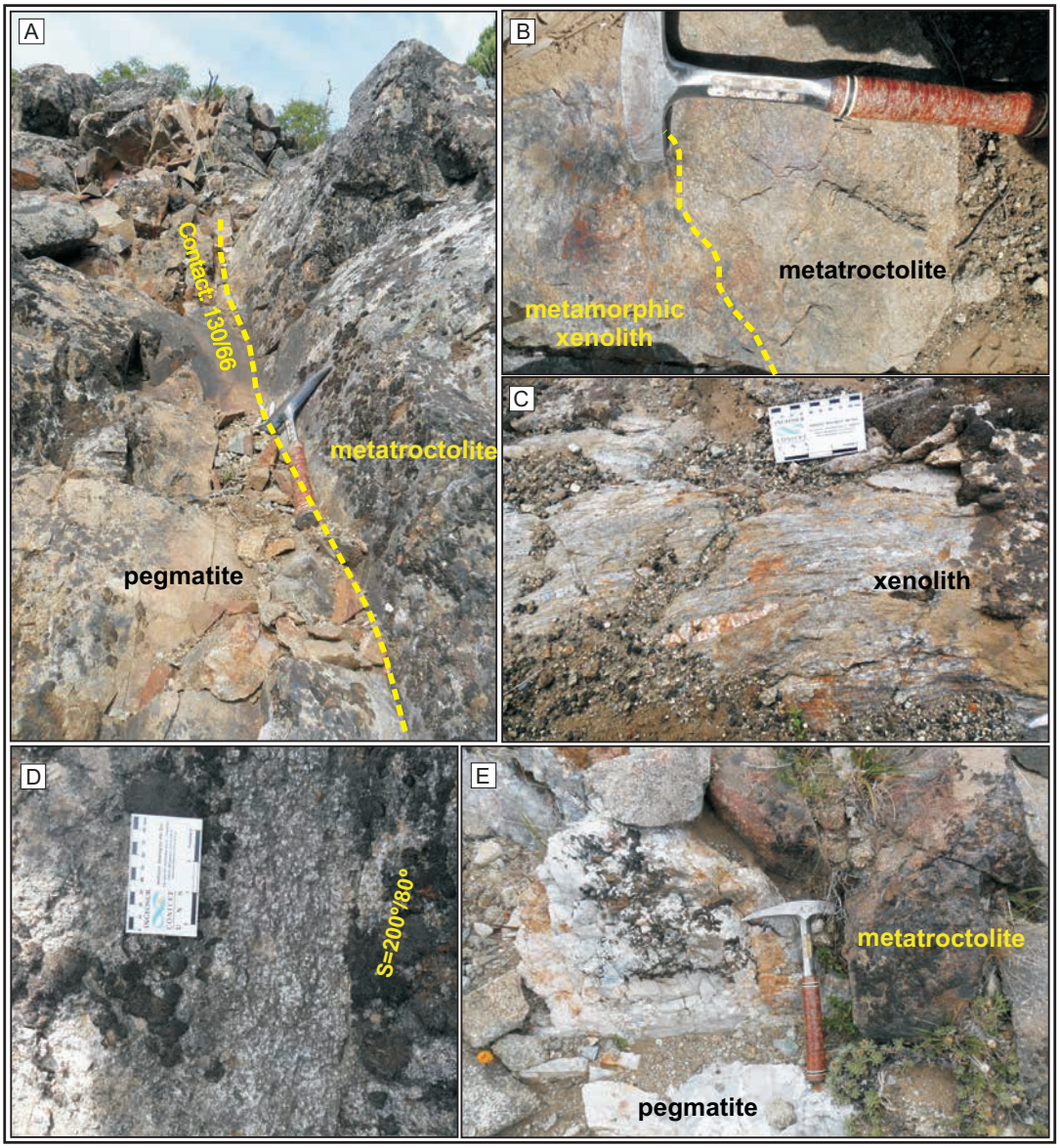

FIG. 3. **A.** Outcrop appearance of the metatroctolites. Note almost massive mafic body, cutting discordantly by an aplitic dike oriented 130º/66°; **B.** Metamorphic xenolith with irregular shape included in the metatroctolite; **C.** Detail of the xenolith. Note the good preservation of the metamorphic fabrica, similar to that observed in the *in situ* exposures of the same contiguous basement rocks; **D.** Rough disjuntive foliation affecting metatroctolites (S=200º/80º); **E.** Pegmatite composed of K-feldspar, quartz and tourmaline megacrystals, cutting the mafic body.

total alkalis of up 4.44% would correspond to more evolved facies. Compared with the metatroctolites, these rocks are richer in iron (X_{Mg}=0.41-0.47) and TiO_2 (1.22-2.55%).

The REE plot in figure 4C, shows a relatively high concentration of LREE and depletion in HREE. The metatroctolites show a strong positive europium anomaly, suggesting the accumulation of plagioclase segregated from the melt. The enrichment of LREE can be explained as the result of contamination from the metasedimentary xenoliths incorporated by the mafic magma. In figure 4C, this rock pattern is

TABLE 1. REPRESENTATIVE MAJOR (WT %) AND REE (PPM) WHOLE-ROCK ANALYSES.

	Metatroctolite	Gabbroid inclusion	Gabbronorite
SiO_2	43.1	48.4	51.7
Al_2O_3	19.7	18.5	19.8
FeO	10.6	12.0	8.3
MnO	0.14	0.24	0.17
MgO	14.7	4.7	4.1
CaO	11.6	8.1	8.7
Na_2O	0.61	3.91	4.04
K_2O	0.10	0.23	0.40
TiO_2	0.07	2.55	1.22
P_2O_5	0.01	0.78	0.37
LOI	0.33	0.85	0.06
Total	**101**	**100.2**	**99.67**
La (ppm)	1.27	17.80	14.80
Ce	2.49	44.00	33.60
Pr	0.29	6.44	4.60
Nd	1.18	32.50	19.20
Sm	0.30	8.82	4.80
Eu	0.17	1.95	1.78
Gd	0.33	9.94	4.63
Tb	0.06	1.65	0.65
Dy	0.34	9.41	3.65
Ho	0.07	1.85	0.73
Er	0.21	5.18	2.25
Tm	0.03	0.75	0.32
Yb	0.21	4.59	1.94
Lu	0.03	0.72	0.30

compared with the REE diagrams corresponding to gabbronorites and gabbroic inclusions in cretaceous granodiorites (see section 8). The pattern is almost parallel to that of gabbronorites, although this last one shows a major enrichment in total REE. On the other hand, gabbroic xenoliths in granodiorites show total REE similar to gabbronorites, but differ from them by the presence of a slight negative europium anomaly (Fig. 4C).

On the base of the modal composition mafic rocks can be classified as troctolites (Fig. 4A), whereas according to its chemical composition as perido-gabbros (Fig. 4B).

6. Petrography

The Ñorquinco metatroctolites show a coarse granular texture (Figs. 5A and B), and variable proportions of preserved igneous and late magmatic/subsolidus metamorphic minerals. Relict magmatic olivine crystals are usually fractured and normally exceed 500 μm in size. Magnetite appears filling internal microfractures and in the crystals rims. The most conspicuous characteristic showed by relict olivine crystals is the formation of reaction coronas around it, which are composed mainly of pyroxene, amphibole and spinel.

Plagioclase appears either as relict magmatic crystals of the original mineralogy (Pl_1), or filling fractures (Pl_2).Its presents deformation twins and rounded rims when it is in contact with amphibole. The orthopyroxene is mainly present in the reaction coronas, although a few magmatic big interstitial crystals were recognized in some thin sections. Magmatic clinopyroxene (Cpx_1) appears as small relict crystals surrounded by other phases (Fig. 6B and D) Cpx_2 forms part of the coronas around olivine and plagioclase crystals, sometimes forming symplectitic intergrowths with spinel. The presence of orthopyroxene and Cpx_2+Spl symplectites developed around olivine crystals can be attributed to the typical reaction: Pl+Ol⇆Cpx+Opx+Spl. These coronas and the presence of different types of amphiboles, allow tracking the succession of events that affected to the mafic rock following its emplacement. Hbl_1 name is assigned to the oldest recognized crystals of amphibole, which was initially in contact with relict Pl_1 and Ol (Figs. 5C and D). Hbl_2 is characterized by big interstitial crystals, which replace Hbl_1 as well as all of the other constituents of the rock. Green spinel is disseminated everywhere inside the rock and forms part of the previously mentioned symplectites (Fig. 6A, B and C). The formation of coronas and retrograde interstitial mineral association can be represented by the general reaction: Pl_1+Ol+Cpx_1+Hbl_1+H_2O⇆ Opx+Cpx_2+Hbl_2+Pl_2+Spl. Excess of H_2O needed for the reaction, can be either attributed to a late magmatic origin, or to an external incorporation. The metatroctolites are carriers of an important sulfide mineralization, represented principally by pyrrotine, pentlandite and chalcopyrite. These ore minerals were also found filling fractures in the adjacent country rocks.

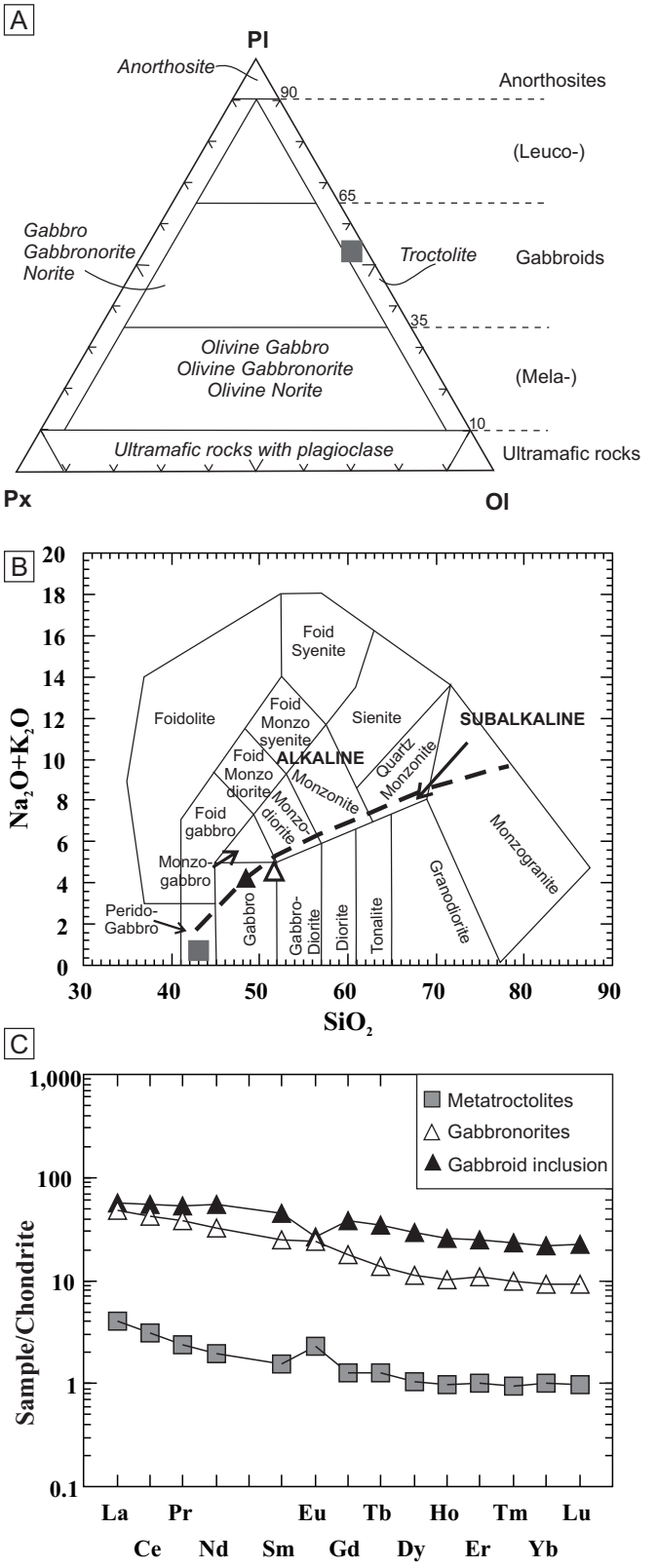

FIG. 4. **A.** Modal classification based on the proportions of plagioclase, pyroxene and olivine; **B.** TAS Diagram (whole alkalis *versus* silica) of Cox *et al*. (1979), adapted by Wilson (1989) and Middlemost (1994) for plutonic rocks. The studied samples lie inside the subalkaline area, and within the perido-gabbros field; **C.** REE composition of metatroctolites, gabbronorites and gabbroic inclusions in granodiorites normalized to Boynton (1984).

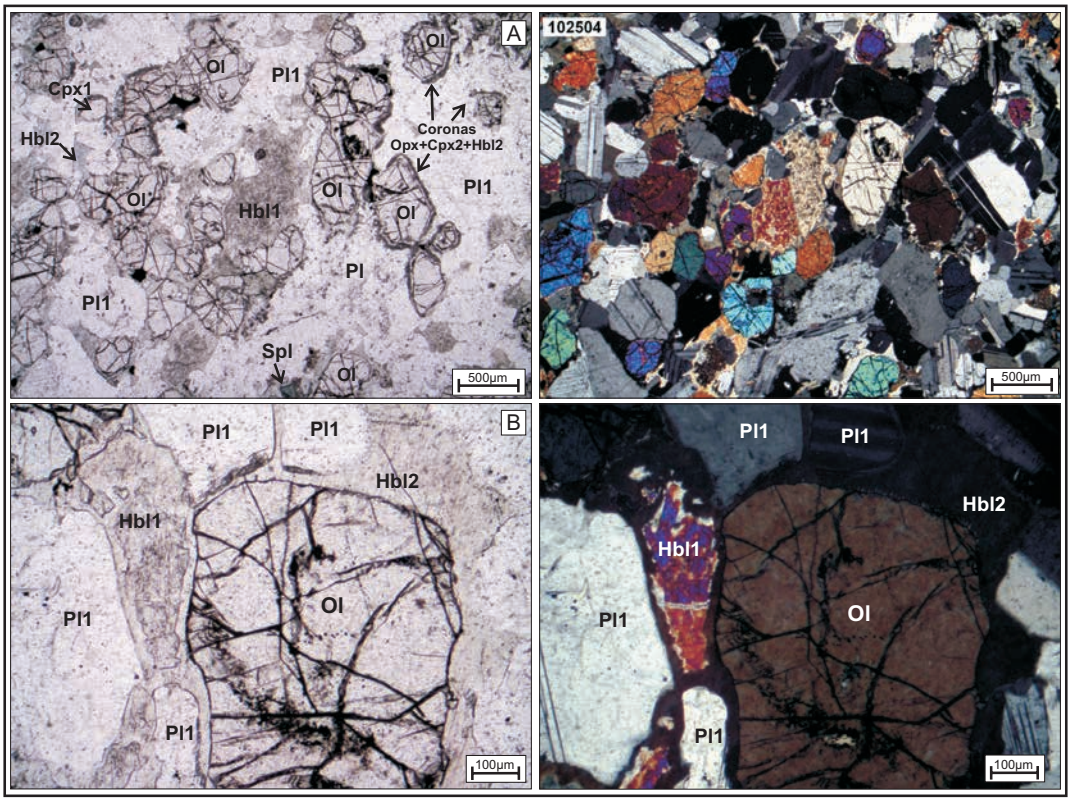

FIG. 5. Parallel light (left) and crossed nicols (right) microphotographs of the metatroctolites. **A.** Granular texture of the metatroctolites formed by big-sized olivine crystals, with development of coronas composed of Opx+Cpx+Hbl_2. Note also the presence of irregular and corroded relict Hbl_1 crystals, surrounded by Hbl_2 and small Spl crystals; **B.** Microphotograph showing replacement of Hbl_1 (initially in 'normal' contact with magmatic plagioclase and olivine), by widespread interstitially distributed Hbl_2.

7. Mineral Chemistry

The chemical compositions of the metagabbro mineral phases present in the metatroctolite were analyzed using a microprobe JEOL 8200 from the Earth and Atmospheric Sciences laboratory of the Alberta University, Canada. The analytical conditions were 15kV accelerating voltage, beam current of 15nA and 3-5 µm spot size. Analyses representative of the different mineral phases and their structural formulas, are presented in Table 2.

7.1. Olivine

It appears as a primary magmatic mineral bordered by reaction coronas composed of pyroxenes and amphiboles. The composition of olivine varies from Fo_{69} to Fo_{73}. Olivine shows only negligible compositional variations between crystals cores and rims.

7.2. Plagioclase

Plagioclase forms part of the original magmatic association of the metatroctolites. It is characterized by high An contents, which varies between 89.2% and 95.6% (Table 2) and lies in the Anorthite field when plotted on the ternary diagram Ab-An-Or (Fig. 7B). Both petrographycally and geochemically is possible to recognize two generation of plagioclase: as phenocrystals (Pl_1) and interstitially (Pl_2). The composition of Pl_1 is fairly uniform, varies between An_{89}-An_{90}, while Pl_2 is substantially more calcium -rich (An_{96}).

7.3. Orthopyroxene

This phase appears in the reaction coronas developed between olivine and plagioclase. Classification of orthopyroxene was carried out using

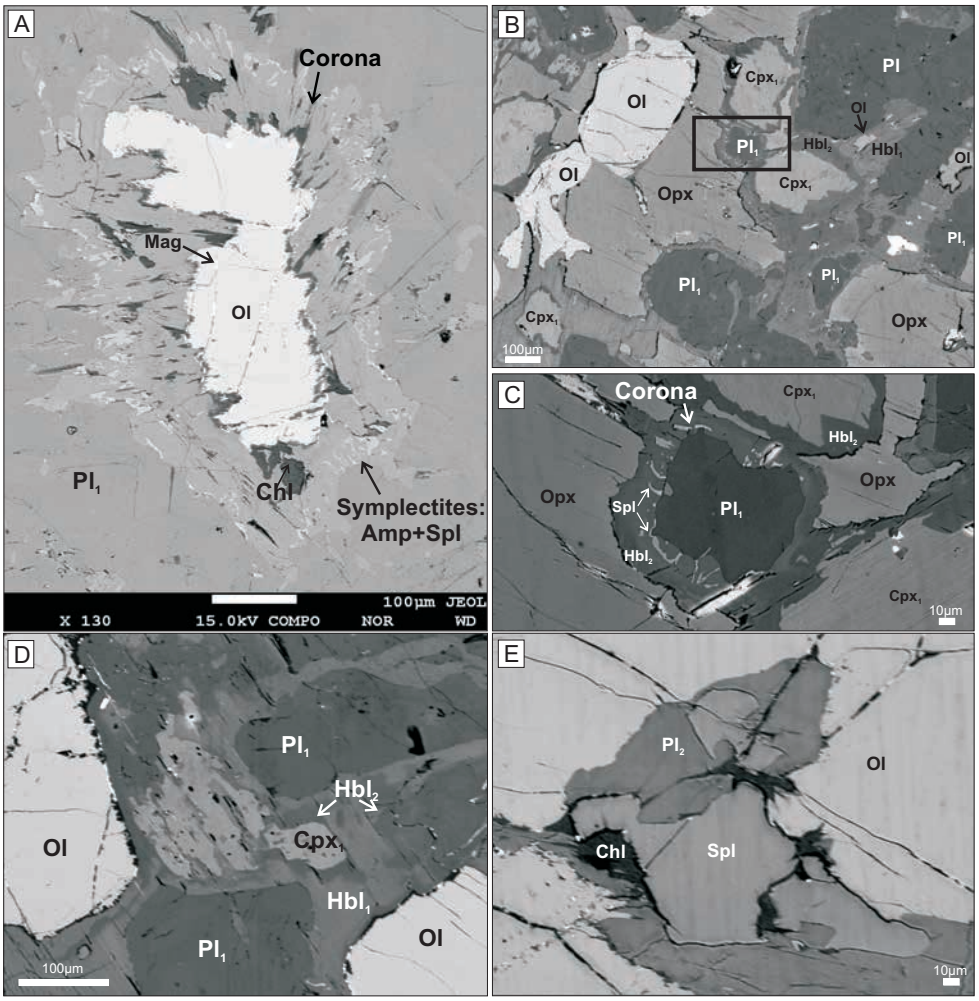

FIG. 6. BSE images of coronas and replacement textures observed in the metatroctolites of Ñorquinco lake. **A.** Amphibole-spinel corona developed around a relict-magmatic olivine crystal. Note symplectitic intergrowth of both minerals towards the external edge of the corona, against plagioclase. Note also, late chlorite and magnetite along olivine-corona contact and filling microcracks; **B.** Interstitial orthopyroxene replacing olivine, plagioclase and clinopyroxene. Observe also, olivine, plagioclase, clinopyroxene and orthopyroxene replaced in a first stage by Hbl_1 and in a second stage by Hbl_2; **C.** Enlargement of the sector delimited by the rectangle in b, showing a Spl-Hbl_2 symplectitic corona developed around a relict-magmatic plagioclase. Note that symplectites develop towards orthopyroxene crystal, and not to the contact with the other phases; **D.** Olivine, plagioclase and clinopyroxene first replaced by Hbl_1 and then by Hbl_2; **E.** Interstitial spinel between plagioclase and olivine. The presence of spinel is attributed to reactions in which these two later phases are the reactants (details in the text). Note also the presence of retrograde chlorite, either interstitial or filling-cracks.

the triangular diagram En-Fs-Wo (Fig. 7C). The proportion of enstatite (En) and ferrosilite (Fs) varies between 69% and 73% ($X_{Mg\ 77}$), whereas the wollastonite component does not overcome 5% for any crystal (Table 2). Orthopyroxene crystals in the metatroctolites have predominantly magnesian compositions, and lie in field of broncite.

7.4. Clinopyroxene

Chemical composition of clinopyroxene crystals (Fig. 7D), can be expressed in terms of the relative proportion of the clinoenstatite-clinoferrosilite-wollastonite components. The analyzed grains indicate that clinopyroxenes are calcium-magnesium

TABLE 2. REPRESENTATIVE CHEMICAL COMPOSITIONS OF THE ORIGINAL-MAGMATIC MINERALS AND PHASES PRODUCED BY DIFFERENT POST-EMPLACEMENT REACTIONS RECOGNIZED IN THE METATROCTOLITES FROM ÑORQUINCO LAKE.

Mineral Sample	Ol 152	Ol 156	Ol 188	Ol 191
SiO_2	38.49	38.67	37.53	38.01
TiO_2	0.00	0.03	0.00	0.01
Al_2O_3	0.01	0.02	0.00	0.00
FeO	25.99	25.03	30.31	27.88
MnO	0.00	0.00	0.02	0.01
MgO	37.16	38.01	33.04	35.34
CaO	0.01	0.04	0.01	0.03
Na_2O	0.39	0.30	0.07	0.29
K_2O	0.01	0.00	0.02	0.06
Total	102.07	102.1	101.01	101.63
Si	0.998	0.997	1.004	1.000
Al	0.000	0.001	0.000	0.000
Ti	0.000	0.001	0.000	0.000
Fe^{2+}	0.565	0.536	0.678	0.613
Fe^{3+}	0.003	0.004	0.000	0.000
Mn	0.000	0.000	0.000	0.000
Mg	1.437	1.461	1.317	1.386
Ca	0.000	0.001	0.000	0.001
Fe/Fe+Mg	0.28	0.27	0.34	0.31
Mg/Fe+Mg	0.72	0.73	0.66	0.69
Numbers of ions on the basis of 4 Oxigens				

Mineral Sample	Pl 1 161	Pl 1 166 Pl4	Pl 1 194	Pl 2 (int) 198 int
SiO_2	45.59	45.09	44.54	43.83
TiO_2	0.03	0.01	0.02	0.03
Al_2O_3	34.79	34.67	34.88	35.82
FeO	0.15	0.35	0.18	0.06
MnO	0.01	0.02	0.00	0.00
MgO	0.26	0.05	0.02	0.00
CaO	18.53	18.70	18.78	19.56
Na_2O	1.23	1.08	1.19	0.50
K_2O	0.01	0.01	0.04	0.00
Total	100.6	99.99	99.65	99.79
Si	8.369	8.341	8.274	8.129
Al	7.521	7.553	7.631	7.824
Ti	0.004	0.002	0.002	0.004
Fe^{2+}	0.023	0.055	0.028	0.009
Mn	0.002	0.003	0.000	0.000
Mg	0.070	0.015	0.006	0.000
Ca	3.645	3.706	3.738	3.887
Na	0.438	0.387	0.427	0.179
K	0.003	0.003	0.01	0
Ab	10.7	9.4	10.2	4.4
An	89.2	90.5	89.5	95.6
Or	0.1	0.1	0.2	0
Numbers of ions on the basis of 32 Oxigens				

Mineral Sample	Opx 153	Opx 160	Opx 163
SiO_2	55.25	54.72	54.88
TiO_2	0.02	0.03	0.02
Al_2O_3	1.89	2.00	1.92
FeO	14.82	14.89	14.74
Cr_2O_3	0.04	0.01	0.02
MgO	27.80	27.52	27.36
CaO	1.06	1.06	1.18
Na_2O	0.07	0.11	0.07
K_2O	0.00	0.00	0.05
Total	100.96	100.33	100.23
TSi	1.962	1.956	1.964
TAl	0.038	0.044	0.036
M1Al	0.041	0.04	0.045
M1Ti	0.001	0.001	0
M1Mg	0.957	0.959	0.953
M2Mg	0.514	0.507	0.507
$M2Fe^{2+}$	0.44	0.445	0.441
M2Ca	0.04	0.041	0.045
M2Na	0.005	0.007	0.005
WO	2.066	2.078	2.319
EN	75.389	75.121	75.011
FS	22.545	22.801	22.67
Mg/Fe+Mg	0.77	0.77	0.77
Numbers of ions on the basis of 6 Oxigens			

Mineral Sample	Cpx 1 222	Cpx 1 236	Cpx 1 155
SiO_2	53.58	53.25	53.14
TiO_2	0.15	0.17	0.24
Al_2O_3	1.54	1.44	2.30
FeO	5.43	4.82	5.76
Cr_2O_3	0.13	0.19	0.32
MgO	15.93	15.60	15.65
CaO	22.95	23.70	22.53
Na_2O	0.22	0.04	0.16
K_2O	0.01	0.03	0.01
Total	99.94	99.27	100.11
TSi	1.97	1.97	1.95
TAl	0.03	0.03	0.05
M1Al	0.03	0.03	0.05
M1Ti	0.00	0.01	0.01
M1Fe2+	0.09	0.09	0.08
M1Mg	0.87	0.86	0.86
M2Fe2+	0.08	0.06	0.10
M2Ca	0.90	0.94	0.89
M2Na	0.02	0.00	0.01
WO	46.50	48.19	46.16
EN	44.91	44.13	44.61
FS	8.59	7.68	9.23
Mg/Fe+Mg	0.84	0.85	0.83
Numbers of ions on the basis of 6 Oxigens			

Chemical mineral analyses expressed as oxide weight %.

Mineral Sample	Spl 183	Spl 195	Spl 217
SiO_2	0.03	0.08	0.03
TiO_2	0.01	0.02	0.00
Al_2O_3	64.72	64.35	65.96
FeO	22.63	21.64	21.47
MnO	0.019	0.011	0.007
MgO	13.16	13.45	13.87
CaO	0.015	0.017	0.026
Na_2O	0.012	0.166	0.223
K_2O	0.00	0.06	0.02
Total	100.59	99.79	101.6
Si	0.001	0.002	0.001
Al	1.991	1.99	1.997
Fe^{2+}	0.494	0.475	0.462
Mg	0.513	0.526	0.532
K	0.000	0.002	0.001
Fe/Fe+Mg	0.49	0.47	0.46
Mg/Mg+Fe	0.51	0.53	0.54
Numbers of ions on the basis of 4 Oxigens			

Mineral Sample	Hbl 1 169	Hbl-1 192	Hbl-1 227
SiO_2	45.33	44.97	46.84
TiO_2	0.359	0.358	0.434
Al_2O_3	12.24	14.62	11.35
FeO	7.24	7.3	7.78
Cr_2O_3	0.092	0	0
MnO	0	0	0.502
MgO	16.17	15.73	16.36
CaO	11.78	11.62	12.21
Na_2O	1.92	2.21	1.87
K_2O	0.649	0.188	0.544
Total	95.69	97	97.89
TSi	6.53	6.35	6.63
TAl	1.47	1.65	1.37
CAl	0.61	0.79	0.52
CFe^{3+}	0.48	0.63	0.44
CTi	0.04	0.04	0.05
CMg	3.47	3.31	3.45
CFe^{2+}	0.39	0.24	0.48
BCa	1.82	1.76	1.85
BNa	0.18	0.24	0.15
ANa	0.35	0.36	0.37
AK	0.12	0.03	0.10

Mineral Sample	Hbl 2 171	Hbl 2 181	Hbl 2 223	Tr 221	Tr 226
SiO_2	46.98	45.74	46.37	55.62	55.16
TiO_2	0.341	0.252	0.382	0.033	0.08
Al_2O_3	11.630	11.870	11.800	1.578	2.54
FeO	7.08	8.9	8.73	5.22	5.07
Cr_2O_3	0.023	0.071	0.109	0.013	0.206
MnO	0	0	0	0.01	0
MgO	16.67	15.65	15.84	21.88	20.97
CaO	12.82	12.2	12.52	11.85	12.21
Na_2O	1.57	1.72	1.77	0.364	0.633
K_2O	0.691	0.889	0.649	0.025	0.044
Total	97.78	97.22	98.06	96.58	96.71
TSi	6.66	6.55	6.58	7.65	7.64
TAl	1.34	1.45	1.42	0.26	0.36
CAl	0.60	0.56	0.56	0.09	0.00
CFe^{3+}	0.22	0.44	0.35	0.00	0.05
CTi	0.04	0.03	0.04	0.51	0.47
CMg	3.52	3.34	3.35	0.00	0.01
CFe^{2+}	0.62	0.62	0.69	4.49	4.33
BCa	1.95	1.87	1.91	0.00	0.12
BNa	0.05	0.13	0.10	1.75	1.81
ANa	0.38	0.35	0.39	0.10	0.17
AK	0.13	0.16	0.12	0.00	0.01
Numbers of ions on the basis of 23 Oxigens					

Mineral Sample	Chl 189	Chl 197	Chl 219
SiO_2	29.58	29.10	30.63
TiO_2	0.01	0.00	0.00
Al_2O_3	21.54	21.36	21.95
FeO	8.01	7.55	7.33
MnO	0.01	0.01	0.02
MgO	28.30	26.93	31.57
CaO	0.01	0.02	0.01
Na_2O	0.18	0.45	0.00
K_2O	0.02	0.06	0.01
Total	87.66	85.48	91.52
Si	5.659	5.701	5.595
Al^{IV}	2.341	2.299	2.405
Al^{VI}	2.512	2.629	2.316
Ti	0.002	0.000	0.000
Fe^{2+}	1.282	1.237	1.120
Mn	0.001	0.001	0.003
Mg	8.071	7.865	8.596
Ca	0.002	0.004	0.002
Na	0.068	0.171	0.000
K	0.004	0.014	0.003
Fe/Fe+Mg	0.14	0.14	0.12
Mg/Fe+Mg	0.86	0.86	0.88
Numbers of ions on the basis of 36 Oxigens			

Mineral formula calculated with the program Minpet, v2.02 (Richard, 1995).

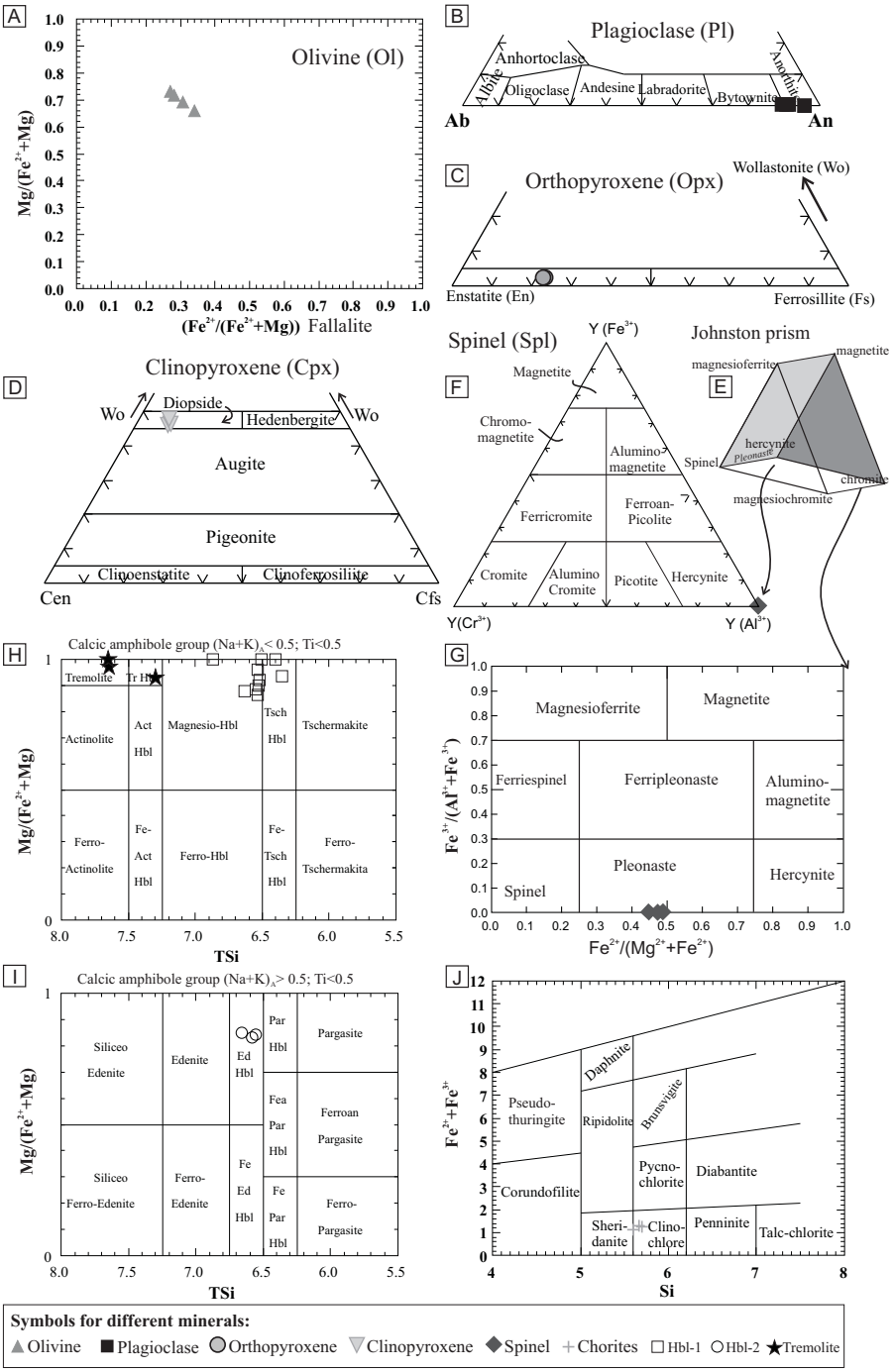

FIG. 7. **A.** Olivine classification diagram (isomorphic binary series forsterite-fayalite, based on the Mg/Mg+Fe^{2+} and Fe^{2+}/Fe^{2+}+Mg proportions; **B.** Ab-An-Or ternary diagram; **C.** Ternary diagram for orthopyroxene classification. Observe the intermediate compositions of the isomorphic series between the end-members enstatite (En) and ferrosilite (Fs); **D.** Ternary diagram for classification of clinopyroxene. Note the intermediate compositions of the isomorphic series between the extremes clinoenstatite (Cen) and clinoferrosilite (Cfs); **E.** Prism of Jhonston for classification of spinel group minerals; **F.** Triangular diagram of trivalent cations (Fe^{3+}-Cr^{3+}-Al^{3+}); **G.** Diagram of spinel classification according to the relative proportions of bivalent and trivalent ions; **H.** Classification of calcic amphiboles [(Na+K)<0.5, Ti<0.5] according to Leake *et al*. (1997); **I.** Classification of calcic amphiboles [(Na+K)>0.5, Ti<0.5] according to Leake *et al*. (1997); **J.** Chlorite classification diagram (taken from Deer *et al*., 1992).

diopsides, with a wollastonitic component varying between is 46.16%-48.19%, and $X_{Mg\ 83\text{-}85}$ (Table 2). Cpx_1 is the relict phases, although scarce Cpx_2 is found only in coronas.

7.5. Spinel

Pure end-members of the spinel group are rarely found in nature. They can be subdivided on the base of their dominant divalent and trivalent cations. The compositions of the multicomponent system of the spinel group, can be plotted on the prism of Johnston (Fig. 7E), whose extremes are given by magnetite, magnesioferrite, spinel, magnesiochromite and chromite (Deer *et al*., 1992). Gargiulo *et al*. (2013) propose classification diagrams based on the faces of the Johnston's prism. Figure 5F, shows a classification of the spinel group based on the exchange of the trivalent cations on the Y position. This classification allows separating the fields of Fe^{3+}-rich spinels representing the magnetite end-member, from the Cr^{3+}-rich and Al^{3+}-rich fields corresponding to chromite and hercynite end-members, respectively. Figure 5G, shows that the analyses individuals have intermediate compositions between spinel and hercynite, with most of them being located within the pleonaste field. Only one analysis lies on the spinel field, which corresponds to aSpl-Hbl symplectite developed in the contact between olivine and plagioclase crystals (Fig. 6 A-C).

7.6. Amphiboles

Three generations of amphiboles were recognized in the metatroctolites. The first two classify as hornblendes (Hbl_1, Hbl_2) and the third as tremolite (Tr). According to Leake *et al*. (1997), Hbl_1 classifies as magnesium-hornblende, although most of them lie on the limit with the tchermarkitic-hornblende field as shown in figure 4G. The petrographic analysis shows that Hbl_1 is replaced by Hbl_2, whose composition corresponds to an edenite-hornblende (Fig. 7H). The tremolitic amphibole, replaces the olivine crystals and the minerals forming the reactions coronas, and clearly corresponds to a very late-low temperature retrogression.

7.7. Chlorite

Chlorites are magnesian and classify as chlinoclores in the Si *versus* (Fe^{3+}+Fe^{2+}) diagram (Deer, 1992) (Fig. 7I). Like tremolites, chlorites correspond to a late-low temperature alteration event.

8. Mineral re-equilibration

The sequence of mineral re-equilibrations in metatroctolites from Ñorquinco lake is shown in Table 3. The original igneous association is constituted by Ol+Pl_1+Cpx_1. First replacement textures are represented by the growth of Opx on Cpx_1 crystals (stage A in Table 3). The appearance of Hbl_1 due to hydration of the previous phases form the association corresponding to stage B. Spl, Hbl_2 and Pl_2 formed during stage C. Stage D is characterized by the late formation of Tr and Chl.

8.1. Stage A formation of Orthopyroxene

Orthopyroxene is the first mineral representing replacement textures in the metatroctolites. It clearly replace the igneous minerals Ol-Cpx_1. Convex grain boundaries towards olivine in Ol-Opx contacts, indicate growth of orthopyroxene at the expense of olivine crystals.

8.2. Stage B formation of Mg-Hornblende (Hbl_1)

The development of amphibole (Hbl_1) is the result of the reaction between Ol-Cpx_1 and Pl_1 with the progressive increase in H_2O concentration. The widespread occurrence of Hbl_1 generates lobed edges

TABLE 3. MINERALOGICAL EVOLUTION OF ÑORQUINCO METATROCTOLITES FOLLOWING THE MICROSTRUCTURAL RELATIONSHIPS.

Stage	relict igneous association	Post-emplacement evolution			
		A	B	C	D
Ol	Ol_1				
Pl	Pl_1 ($An_{89\text{-}90}$)			Pl_2 (An_{96})	
Cpx	Cpx_1			Cpx_2	
Spl				Spl	
Opx		Opx			
Hbl_1			Hbl_1		
Hbl_2				Hbl_2	
Tr					Tr
Chl					Chl

around Pl, and sometimes full replacement of Ol, although some small remnants of Ol with irregular borders were found. It is not possible to recognize close contacts between Ol and Pl because Hbl_1 is always present between these original phases.

8.3. Stage C: formation of Mg-Hornblende (Hbl_2), Spinel and Cpx_2

As a result of the progressive changes in the physical conditions, a new amphibole (Hbl_2) replacing the pre-existing phases is formed. Spl generates symplectites with Hbl_2 around Ol and Pl. Hbl_2 replaces Hbl_1 and forms reaction rims around Cpx-Hbl_1 and Opx-Hbl_1. Cpx_2 was recognized in some coronas associated with Spl. Hbl_2 and Spl form symplectites around relict phases.

8.4. Stage D: formation of Chl-Tr

The formation of Chl and Tr in very low proportions is attributed to the last stage of retrogression. Chl is mainly replacing the different phases of the corona and surrounding olivine. Magnetite filling fractures inside olivine crystals, is also assigned to this stage.

9. Phase relations, geothermobarometry and P-T path

In order to evaluate the stability of the observed mineral associations, a suitable P-T pseudosection was constructed with the program Perplex_X (Connolly, 1990, version 2013). The diagram was calculated using the whole-rock chemistry of the metatroctolites (Fig. 8), considering the chemical system Na_2O-CaO-FeO-MgO-Al_2O_3-SiO_2-H_2O and including the following phases: plagioclase, olivine, orthopyroxene, clinopyroxene, spinel, amphibole, garnet, chlorite and water. The solid solution models for olivine, clinopyroxene, orthopyroxene garnet, spinel and chlorite correspond to Holland and Powell (1998, and updated versions); for plagioclase and amphibole were used the formulations of Newton *et al*. (1980) and Dale *et al*. (2005), respectively.

Pseudosection analysis was complemented with the application of classical geothermobarometry to selected mineral pairs. Using the Opx-Cpx_1 geothermometer of Wood and Banno (1973) and the Cpx_1-Pl geobarometer of Kretz and Jen (1978), a temperature of 936 ºC and a pressure of 2.7 Kb were obtained (Table 4). This point, when plotted on the pseudosection (A) of figure 8, locates within the stability field of the association Ol+Pl_1+Cpx_1+Opx+H_2O. Possibly, there was not available free water during this first stage, but the incorporation of this fluid component is necessary in order to generate the hydrated phases observed. This free water might have been originated during late magmatic crystallization, supplied by an external source, or by a combination of both provenances. Point A is considered to be the nearest condition to the reached metamorphic peak by the metatroctolites, and it is established as the starting point for the post-emplacement trajectory.

The conditions of the point B in figure 8, were calculated through the geothermometer TB of Holland and Blundy (1994), using the mineral pair Pl_2-Hbl_1 and the Al-in-Hbl geobarometer of Johnson and Rutherford (1989) for Hbl_1, obtaining a temperature of 851 ºC and a pressure of 4.26 Kb. Point B lies in the stability field of the association Ol+Pl+Cpx+Opx+Hbl_1+H_2O, and differs from the previous one for the first appearance of the amphibole (Hbl_1). The trajectory between points A and B implies increasing pressures and decreasing temperatures, and requires of the availability of free water to form amphibole. The P-T condition of stage B is well constrained by the compositional isopleths of X_{Mg} in Opx (0.77), as well as in Cpx X_{Mg}=0.85 (Fig. 9A, B). Anorthite proportions in Pl for the stage B is around (X_{Ca}=0.96), whose composition is the same as that obteined for Pl_2 with microprobe analysis. X_{Si} in amphibole varies between 6.5 and 6.6 (a.p.f.u) (Fig. 9 C and D). The estimated isopleths are fully coincident with the P-T conditions obtained for stage B using classical geothermobarometry.

Textural relationships indicate that Hbl_1 is replaced by the Hbl_2, which indicates a new stage of mineralogical re-equilibrium. Applying the same thermometer and geobarometer to Pl_2-Hbl_2 pair, a temperature of 780 ºC and a pressure of 5.69 Kb were obtained. This point represented in figure 8 with the letter C, corresponds to the stability field of the mineral association Pl+Cpx+Opx+Amph+Spl+H_2O. The transition from the previous to this stability field carries with it the disappearance of Ol and the appearance of the Hbl_2+Spl pair. Petrography shows that this later phases are always spatially and texturally associated. The appearance of spinel is consistent with petrographic

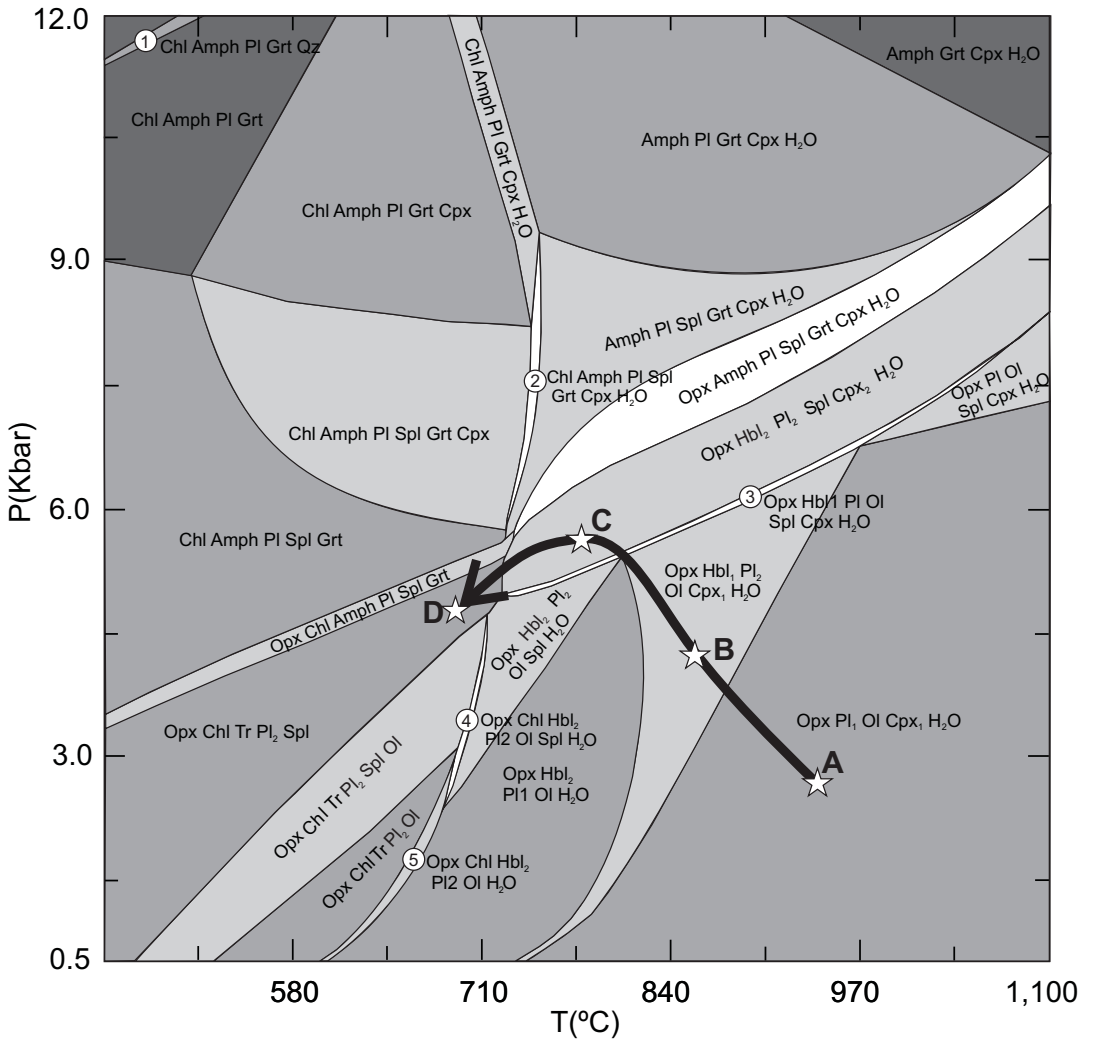

FIG. 8. P-T Pseudosection for the metatroctolites calculated for the system NCFMASH and a whole-rock chemical composition (wt% oxides): SiO_2=43.1; TiO_2=0.068; Al_2O_3=19.7; FeO=9.57; MgO=14.67; CaO=11.62; K_2O=0.1; Na_2O=0.61; H_2O=1.5. The points A, B, C and D have been obtained through classical geothermobarometry applied to different mineral pairs.

observations, which indicates the development of the reaction Ol+Pl⇆Opx+Cpx+Spl, typical of these rock types. Given that reaction Spl+Px⇆Grt+Ol, which fixes the upper pressures limit for the stability of the association listed above, did not take place considering the total absence of garnet in the studied rocks, point C establishes an approximated maximum for pressures reached by these rocks. The X_{Si} composition in Hbl_2 is around 6.6-6.7 (a.p.f.u), though the stage C calculated using conventional geothermobarometry corresponds to a little high composition X_{Si} 6.9-7.0 for the isopleths (Fig. 9D).

Finally, the presence of chlorite allows estimation of a temperature of 694 ºC, calculated with the formulation Al-in-Chl of Cathelineau (1988). According to pseudosection of figure 8, the formation of chlorite is associated to the total consumption of water and clinopyroxene present in the previous paragenesis, giving place to the new stable association Pl+Opx+Amp+Spl+Chl. Considering the calculated temperature for chlorite, a range of pressures can be estimated considering the absence of olivine in the above listed association which fix a minimum pressure at ~4.5 Kb, and the entire absence

TABLE 4. GEOTHERMOBAROMETRIC RESULTS OBTAINED FROM THE APPLICATION OF THE DIFFERENT FORMULATIONS INDICATED, TO SEVERAL MINERAL PHASES.

Geothermometers		T (ºC)	Geobarometers		P (Kbar)
Opx-Cpx1	Wood and Banno (1973) P=2.7	933	Cpx1-Pl1	Ellis (1980) T=933 ºC	2.7
	Putirka (2008) Eqn 36	939		Ellis (1980) T=939 ºC	2.63
	Average	936		Average	2.67
Pl-Hbl			Al in Hbl		
Mg-Hbl (Hbl 1)	Holland and Blundy (1994) TB	823	Mg-Hbl (Hbl-1)	Johnson and Rutherford (1989)	4.26
Ed-Hbl (Hbl 2)	Holland and Blundy (1994) TB	780			
Cpx1- Hbl 1	Kretz and Jen (1978)	880	Al in Hbl		
	Average Pl-Hbl 1 and Cpx1- Hbl 1	851.5	Ed-Hbl (Hbl-2)	Johnson and Rutherford (1989)	5.69
Al in Chl	Cathelineau (1988) Average Chl	694.2			

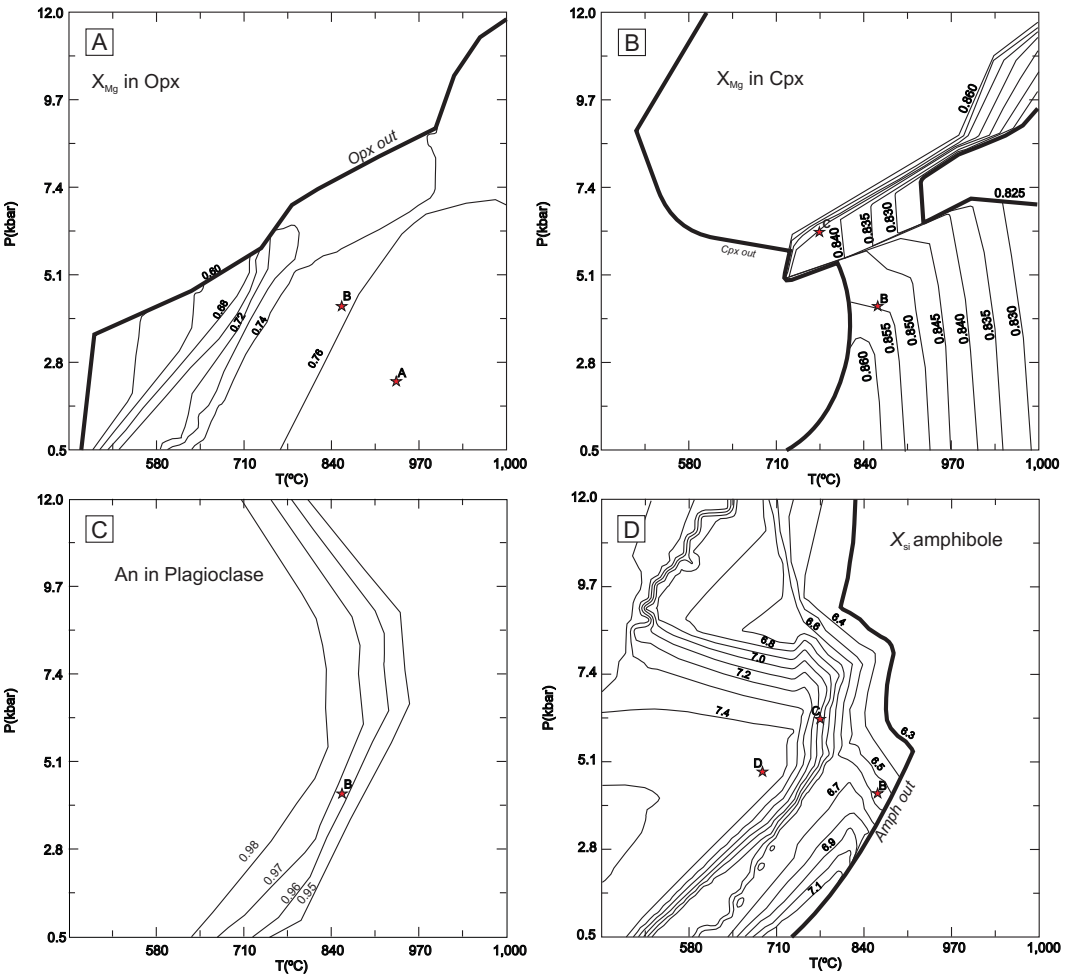

FIG. 9. Compositional isopleths. **A.** X_{Mg} in Orthopyroxene; **B.** X_{Mg} in Clynopyroxene; **C.** An in plagioclase; **D.** X_{Si} in amphiboles. The post-emplacement stages B, C and D (showed with stars) are the P-T values calculated with conventional geothermobarometry.

of garnet in these rocks establishing a maximum pressure of ~5.2 Kb (Fig. 8). Letter D in figure 8, is located in the middle of these values and at the calculated temperature. Taking into account that the continuity of the trajectory is limited by the last stability field, the trajectory must continue along a path characterized by the decrease of temperatures and pressures (Fig 8).

10. Estimation of the metatroctolites relative age

The presence of abundant metasedimentary xenoliths from the country-rocks fixes a maximum Late Devonian age (360 Ma, Urraza *et al*., 2009). On the other hand, xenoliths of strongly deformed metagabbros composed of Opx+Pl+Hbl+Bt+Ilm, were found included in granodiorites. In spite of these xenoliths are strongly affected by deformation, they preserve a mineralogical and geochemical composition similar to the studied metatroctolites. In the present contribution, a U-Pb zircon age of 309±31 Ma has been determined for the metagabbroic xenoliths, whereas for the host granodioritic rocks a U-Pb zircon age of 82±1.6 Ma was established (Fig. 10 A and B). Isotopic data were acquired using a Nu Plasma MC-ICP-MS coupled to a laser ablation system. The well-calibrated zircon standard LH-9415 was used as the standard for the normalization of the Pb/U values in the University of Alberta. Simonetti *et al*. (2006) show the advantages of using U-Pb laser ablation for zircon, monazite and titanite grains in standard petrographic thin section and demonstrate the effectiveness of the *in situ* technique in providing accurate and relatively precise age information. A laser beam spot of 40 µm was used; considering it is the appropriate size for Paleozoic rocks. Simonetti *et al*. (2006) mention that it should prove particularly valuable for obtaining U-Pb ages in reconnaissance-type studies, such as preliminary geological studies of regions that contain little or no prior geochronological age information. Therefore, it is an appropriate technique for preliminary information in the AIMC.

The ages found for the country-rock xenoliths and gabbroic inclusions in granodiorites, constrain the metatroctolites formation to Upper Paleozoic times, which allows linking its intrusion to the early stages of gondwanian magmatism.

11. Conclusions

1. Mafic rocks from the north of Ñorquinco lake were classified based on the primary modal composition as metatroctolites, and on the base of the alkalis content as perido-gabbros.
2. The primary-magmatic association composed mainly of Pl_1+Ol+Cpx_1+Hbl_1, was re-equilibrated during the post-emplacement thermal descent giving place to the formation of coronas around olivine crystals, with successive formation of orthopyroxene, clinopyroxene (Cpx_2), amphibole (Hbl_2) and spinel.

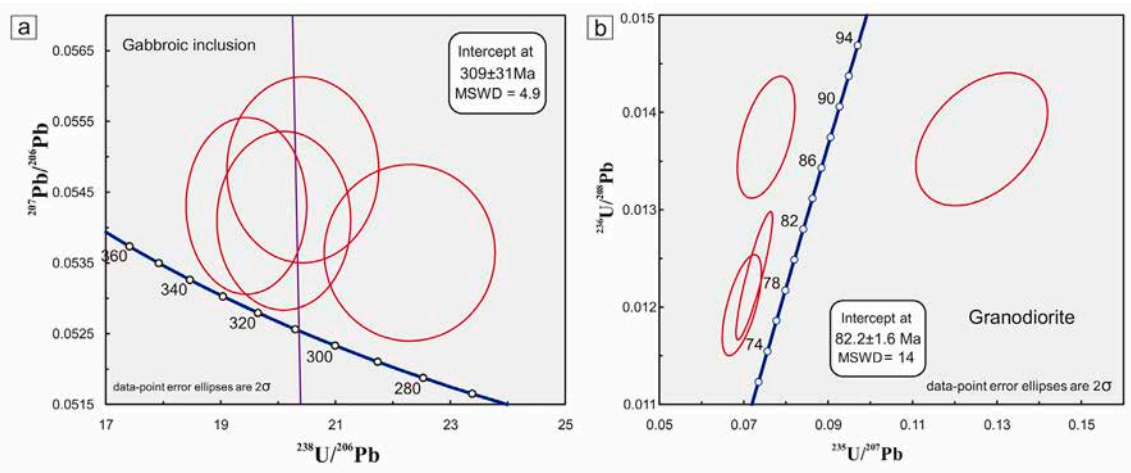

FIG. 10. **A.** Tera-Wasserburg concordia representation of the data obtained from analyzed zircons, using thin section *in situ* LA-ICP-MS with a 40 µm bundle. U-Pb age for gabbroic inclusions in granodiorites; **B.** Wetherill concordia U-Pb age for host granodiorites.

3. The presence of water, either late-magmatic or externally incorporated, gave place to the appearance of high temperature amphiboles (Hbl_1, Hbl_2) and the late lower-temperature phases, chlorite, magnetite and tremolite. These phases formed by the hydration of the primitive anhydrous phases, and crystallized at different stages of the evolution of these rocks.
4. Considered together, textural relationships established via petrographic studies, pseudosection analysis and geothermobarometry, allow us to reconstruct a counterclockwise P-T path for the post-emplacement evolution of the metatroctolite. This trajectory is consistent with the evolution determined for the adjacent country-rocks previously studied by the authors (Urraza *et al*., 2009).
5. Based on the established ages for basement xenoliths in metatroctolites and gabbroic inclusions in granodiorites, the emplacement of the Ñorquinco lake metatroctolites can be constrained to the Upper Paleozoic.

Acknowledgements

This work was financed by funds of the PICT2008 No. 1379 granted to Dra. L. Grecco. We thank Dr. M. Zentilli of Dalhousie University and Dr. L. Heamann of University of Alberta, Canada, where the laboratory works were carried out. We are grateful to Dr. Indares, Dr. Steenken and Dr. Cruciani for the constructive reviews.

References

Ashworth, J.R. 1986. The role of magmatic reaction, diffusion, and annealing in the evolution of coronitic microstructure in troctolitic gabbro from Risör, Norway: a discussion. Mineralogical Magazine 50: 469-473.

Boynton, N.V. 1984. Geochemistry of the rare earth elements: meteorite studies. *In* Rare Earth Element Geochemistry (Henderson, P.; editor). Elsevier: 63-114.

Brogioni, N.; Cruciani, G.; Franceschelli, M.; Vaselli, O. 2007. Evolución metamórfica de los gabros coroníticos de El Arenal, faja máfica-ultramáfica El Destino-Las Águilas, sierra de San Luis. Revista de la Asociación Geológica Argentina 62 (1): 13-24.

Cathelineau, M. 1988. Cation site occupancy in chlorites and illites as a function of temperature. Clay Minerals 23: 471-485.

Claeson, D.T. 1998. Coronas, reaction rims, symplectites and emplacement depth of the Rymmen gabbro, Transscandinavian Igneous Belt, southern Sweden. Mineralogical Magazine 62 (6): 743-757.

Connolly, J.A.D. 1990. Multivariable phase diagrams; an algorithm based on generalized thermodynamics. American Journal of Science 290: 666-718.

Cox, K.G.; Bell, J.D.; Pankhurst, R.J. 1979. The interpretation of igneous rocks. George, Allen and Unwin: 450 p. London.

Cruciani, G.; Franceschelli, M.; Groppo, C.; Brogioni, N.; Vaselli, O. 2008. Formation of clinopyroxene + spinel and amphibole + spinel symplectites in coronitic gabbros from Sierra de San Luis (Argentina): a key to post-magmatic evolution. Journal of Metamorphic Geology 26: 759-774.

Cruciani, G.; Franceschelli, M.; Brogioni, N. 2011. Mineral re-equilibration and P-T path of metagabbros, Sierra de San Luis, Argentina: insights into the exhumation of mafic-ultramafic belt. European Journal of Mineralogy 23: 591-608.

Cruciani, G.; Franceschelli, M.; Brogioni, N. 2012. Early stage evolution of the mafic-ultramafic belt at La Melada, Sierra de San Luis, Argentina: P-T constraints from metapyroxenite pseudosection modelling. Journal of South American Earth Sciences 37: 1-12.

Dale, J.; Powell, R.; White, W.; Elmer, F.L.; Holland, T.J.B. 2005. A thermodynamic model for Ca-Na clinoamphiboles in Na_2O-CaO-FeO-MgO-Al_2O_3-SiO_2-H_2O-O for petrological calculations. Journal of Metamorphic Geology 23 (8): 771-791.

Deer, W.A.; Howie, R.A.; Zussman, J. 1992. An introduction to the rock forming minerals. Engleand Editors. Longamn Scientific and Technical: 695 p. Harlow.

Ellis, D.J. 1980. Osumilite-sapphirine-quartz granulites from Enderby Land, Antartica: P-T conditions of metamorphism, implications for garnet-cordierite equilibria and the evolution of the deep crust. Contributions to Mineralogy and Petrology 74 (2): 201-210.

Hervé, F.; Pankhurst, R.J.; Fanning, C.M.; Calderon, M.; Yaxley, G.M. 2007. The South Patagonian batholith: 150 my of granite magmatism on a plate margin. Lithos 97: 373-394.

Holland, T.; Blundy, J. 1994. Non-ideal interactions in calcic amphiboles and their bearing on amphibole-plagioclase thermometry. Contribution to Mineralogy and Petrology 116: 433-447.

Holland, T.; Powell, R. 1998. An internally consistent thermodynamic data set for phases of petrological interest. Journal of Metamorphic Geology 16 (3): 309-343.

Johnson, M.C.; Rutherford, M.J. 1989. Experimental calibration of the aluminium in-hornblende geobarometer with application to Long Valley caldera (California). Geology 17: 837-841.

Franceschelli, M.; Carcangiu, G.; Caredda, A.M.; Cruciani, G.; Memmi, I.; Zucca, M. 2002. Transformation of cumulate mafic rocks to granulite and re-equilibration in amphibole and greenschist facies in NE Sardinia, Italy. Lithos 63: 1-18.

Gallien, F.; Mogessie, A.; Hauzenberger, C.A.; Bjerg, E.; Delpino, S.; Castro de Machuca, B. 2012. On the origin of multi-layer coronas between olivine and plagioclase at the gabbro-granulite transition, Valle Fértil-LaHuerta Ranges, San Juan Province, Argentina. Journal of Metamorphic Geology 30: 281-301.

Gargiulo, M.F.; Bjerg, E.A.; Mogessie, A. 2013. Spinel group minerals in metamorphosed ultramafic rocks from Río de Las Tunas Belt, Central Andes, Argentina. Geologica Acta 11 (2): 133-148.

Gordon, A.; Ort, M.H. 1993. Edad y correlación del plutonismo subcordillerano en las provincias de Río Negro y Chubut (41º-42º30' LS). *In* Congreso Geológico Argentino, No. 12, Actas 4: 120-127. Mendoza.

Griffin, W.L.; Heier, K.S. 1973. Petrological implications of some corona structures. Lithos 6: 315-335.

Kretz, R.; Jen, L.S. 1978. Effect of temperature on the distribution of Mg and Fe^{2+} between calcic pyroxene and hornblende. Canadian Mineralogist 16: 533-537.

Lang, H.M.; Wachter, A.J.; Peterson, V.L.; Ryan, J.G. 2004. Coexisting clinopyroxene/spinel and amphibole/spinel symplectites in metatroctolites from the Buck Creek ultramafic body, North Carolina Blue Ridge. American Mineralogist 80: 20-30.

Leake, B.E.; Wooley, A.R.; Arps, C.E.S.; Birch, W.D.S.; Birch, W.D.; Gilbert, M.C.; Grice, J.D.; Hawthorne, F.C.; Kato, A.; Kisch, H.J.; Krivivichev, V.G.; Linthout, K.; Laird, J.; Mandarino, J.A.; Maresch, W.V.; Nickel, E.H.; Tock, N.M.S.; Schumacher, J.C.; Smith, D.C.; Stephenson, N.C.N.; Ungaretti, L.; Whittaker, E.; Youzhi, G. 1997. Nomenclature of amphiboles: report of the subcommittee on amphiboles of International Mineralogical Association, commission on new minerals and mineral names. European Journal of Mineralogy 9: 623-651.

Le Maitre, R.W. 1989. A Classification of Igneous Rocks and a Glossary of Terms. Blackwell Scientific Publications, Oxford.

Middlemost, E.A.K. 1994. Naming materials in the magma/igneous system. Earth-Science Reviews 37: 215-224.

Mongkoltip, P.; Ashworth, J.R. 1983. Quantitative estimation of an open-system symplectite-forming reaction: restricted diffusion of Al and Si in coronas around olivine. Journal of Petrology 24: 635-661.

Newton, R.C.; Charlu, T.V.; Kleppa, O.J. 1980. Thermochemistry of the high structural state plagioclases. *In* Geochimica et Cosmochimica, Acta 44: 933-941.

Otamendi, J.E.; Cristofolini, E.; Tibaldi, A.M.; Quevedo, F.I.; Baliani, I. 2010. Petrology of mafic and ultramafic layered rocks from the Jaboncillo Valley, Sierra de Valle Fértil, Argentina: implications for the evolution of magmas in the lower crust of the Famatinian arc. Journal of South American Earth Sciences 29: 685-704.

Putirka, K.D. 2008. Thermometers and Barometers for Volcanic Systems. Reviews in Mineralogy and Geochemistry 69: 61-120.

Ramos, V.A. 1978. Estructura. *In* Relatorio Geología y Recursos Naturales del Neuquén: 99-118.

Richard, L.R. 1995. MinPet: Mineralogical and petrological data processing system, version 2.02. MinPet Geological Software, Quebec. Canada.

Simonetti, A.; Heamman, L.M.; Chacko, T.; Banerjee, N.R. 2006. *In situ* petrographic thin section U-Pb dating of zircon, monazite, and titanite using laser ablation-MC-ICP-MS. International Journal of Mass Spectrometry 253: 87-97.

Turner, S.P.; Stüwe, K. 1992. Low pressure corona textures between olivine and plagioclase in gabbros from Black Hill, South Australia. Mineralogical Magazine 56: 503-509.

Urraza, I.A. 2014. Evolución magmática y tectonometamórfica del Complejo Ígneo-metamórfico Aluminé, Provincia de Neuquén, Argentina. Tesis doctoral (Unpublished), Universidad Nacional del Sur: 221 p. Buenos Aires.

Urraza, I.A.; Grecco, L.; Delpino, S.; Zentilli, M. 2008a. Magmatic and tectonic evolution of the Alumine belt, Patagonian Batholith, Neuquén, Argentina. *In* Québec 2008 GAC-MAC-SEG-SGA Annual Meeting, Session: GS4 - Igneous Petrology, Volcanology and Metamorphic Petrology, Abstract No. 174. Canada.

Urraza, I.A.; Grecco, L.E.; Delpino, S.H.; Arrese, M.L.; 2008b. Determination of rock ages by chemical análisis of Th, U, Pb in the mineral monazite (Ce, La, Th REE, U) PO_4 using EPMA. Institute for Research in Materials. *In* Annual General Meeting and Research Day, Abstracts: p. 36. Halifax.

Urraza, I.; Delpino, S.; Grecco, L.; Arrese, M. 2009. Petrografía, geotermobarometría y geocronología del basamento del sector norte del Batolito Patagónico,

Neuquén, Argentina. *In* Reunión de Tectónica, No. 14, Resúmenes: p. 34. Río Cuarto.

Urraza, I.; Delpino, S.; Grecco, L.; Arrese, M.; Rapela, C.W. 2011. Petrografía y Estructura del Complejo Ígneo-Metamórfico Aluminé, Provincia de Neuquén, Argentina. Andean Geology 38 (1): 98-118. doi: 10.5027/andgeoV38n1-a07.

Urraza, I.; Delpino, S.; Grecco, L. 2012. Evolución post-emplazamiento del gabro troctolítico del Norte de Lago Ñorquinco, Complejo Ígneo-Metamórfico Aluminé, Neuquén, Argentina. *In* Reunión de Tectónica, No. 14, Resúmenes: 156-157. San Juan.

Urraza, I.A.; Grecco, L.; Delpino, S. 2013. Sulfuros de Cu, Fe y Ni asociados a los metagabros troctolíticos del lago Ñorquinco, Complejo Igneo-Metamórfico Aluminé, Neuquén, Argentina. *In* Avances en Mineralogía, Metalogenia y Petrología 2013 (Conte-Grand, A.; Castro de Machuca, B.; Meissl, E.; editors): 261-266.

Vaughan, A.P.M.; Pankhurst, R.J. 2008. Tectonic overview of the West Gondwana margin.Gondwana Research 13: 150-162.

Whitney, D.L.; Evans, B.W. 2010. Abbreviations for names of rock-forming minerals. American Mineralogist 95: 185-187.

Wilson, M. 1989. Igneous Petrogenesis. Unwin Hyman: 466 p. London.

Wood, B.J.; Banno, S. 1973. Garnet-orthopyroxene and orthopyroxene-clinopyroxene relationships in simple and complex systems. Contributions to Mineralogy and Petrology 42: 109-124.

Manuscript received: March 26, 2014; revised/accepted: December 05, 2014; available online: December 09, 2014.